FTU results with the liquid lithium limiter

G. Mazzitelli[1], M. L. Apicella[1], D. Frigione[1], G. Maddaluno[1], M. Marinucci[1], C. Mazzotta[1], V. Pericoli Ridolfini[1], M. Romanelli[2], G. Szepesi[3], O. Tudisco[1] and FTU team·

1) Associazione EURATOM-ENEA sulla Fusione, Centro Ricerche di Frascati, C.P. 65 00044 Frascati, Rome, Italy
2) CCFE/Euratom Association, Culham Science Center, OX143DB, UK
3) CFSA University of Warwick, CV47AL, UK

e-mail contact of main author: mazzitelli@frascati.enea.it

Abstract. Since the end of 2005 most of plasma wall interaction experiments on FTU have been focused on the possible use of liquid lithium as plasma facing material. Liquid lithium limiter is an active method to deposit, during the plasma discharge, a lithium film on the walls with prolonged beneficial effects. Reliable operation with very clean plasmas, very low wall particle recycling, spontaneous peaking of the density profile for line averaged density values $\bar{n}_e$>1.0×10^{20} m^{-3} have been obtained. These results have allowed to extend the density limit at the highest value so far obtained ($\bar{n}_e$=4.0x10^{20} m^{-3} at I_p=0.7 MA and B_T=7.1 T, q_a=5.0, by gas puffing only) and to increase the energy confinement time by almost 50% with respect to the average value of 50 ms of the old ohmic FTU database. An accurate analysis of these plasmas has been carried out by means of a gyrokinetic code to establish the role of collisionality and of the density gradients on the observed phenomenology.

1. Introduction

On FTU, experimental programs are in progress with a liquid lithium limiter (LLL) employing a capillary porous system (CPS) [1,2] to investigate physical and technological aspects related to the use of liquid metal as plasma facing material. The main effect of lithium-coated walls is the nearly complete suppression of D_2 wall recycling and the strong reduction of light impurities such as carbon and oxygen. This is also observed on other machines both in limiter and divertor configuration (T11-M, NSTX, RFX, etc). On FTU, which is a metallic machine operating with a TZM toroidal limiter (98% molybdenum) and a Stainless Steel AISI 304 vacuum chamber, lithization has produced very clean plasmas. Only Li emission lines are visible on UV spectra, while those of Mo, O and other impurities are below the instrument sensitivity. Another effect of lithization is to reduce the plasma instabilities at the plasma edge as evidenced by a strong decrease of the m=2, n=1 tearing mode on FTU [3] and by the quasi-suppression of ELM's activity on NSTX [4]. In all cases, the plasma performance is enhanced in terms of energy confinement time and stored energy.
The most interesting feature, which is peculiar of FTU, is the spontaneous strong peaking of the density profiles for line averaged density values $\bar{n}_e$>1.0×10^{20} m^{-3}, that is associated with the appearance of a MARFE and with the formation of a high density gradient at the plasma edge [3]. This phenomenology has not been observed on the other machines operating in a lower density range.
From the technological point of view, a further progress has been made by changing stainless steel with tungsten as material for the matt wires of CPS structure as documented in a previous work [5]. The good performances in terms of damage resistance and prolonged operating capability have been tested by shifting the plasma directly on the LLL structure for about 300 ms, with average thermal loads up to 5 MW/m^2 and peak values greater than 10MW/m^2 during plasma disruptions.

· See Appendix of A. A. Tuccillo et al., paper OV/4-2, this conference

In this paper, after a brief description of the system, a review of the main experimental results with LLL will be presented, referring to previous papers for more details. More attention will be paid to the formation of highly peaked density discharges, to the enhancement of plasma performances and to the results of a gyrokinetic code accounting for the observed phenomenology. The modifications induced by lithium on the particle transport will be discussed by means of an analysis of the dominant instabilities operating in these plasmas. Finally the conclusions will be drawn.

2. The Liquid Lithium Limiter (LLL)

The lithium limiter (fig.1) employs a CPS configuration already tested successfully on T-11M [6] and it is composed by three separated and electrically insulated modules. Two of them consist of a surface layer of wire meshes of stainless steel 304 with pore radius 15 μm and wire diameter 30 μm while the third module has the wire meshes made of tungsten. The surface facing the plasma is refilled through capillary forces by a liquid lithium reservoir placed at the bottom of this structure.

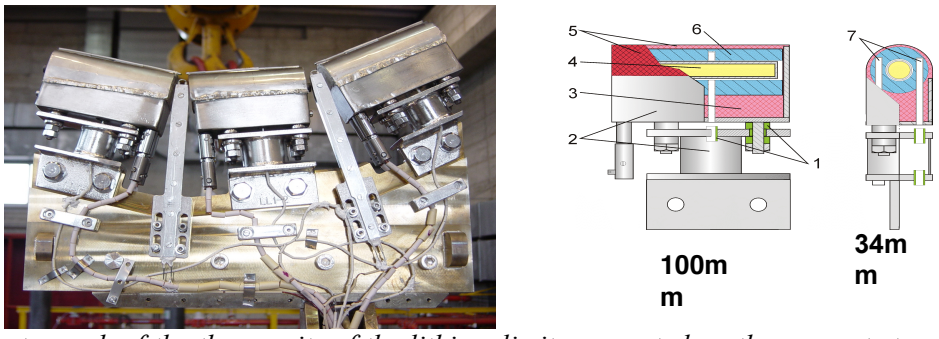

Fig. 1*. Photograph of the three units of the lithium limiter mounted on the support structure used for the introduction inside FTU. The two Langmuir probes are visible in the interspace between units. 1) ceramic break, 2) stainless steel casing, 3) lithium filled-capillary structure, 4) heater, 5) Li evaporating surface 6) Mo heat accumulator, 7) thermocouples*

The LLL is equipped with two thermocouples for each module and two Langmuir probes placed in between the modules to characterize the scrape-off plasma near the limiter surface. Infrared detectors look at the three modules to monitor the lithium surface temperature during the discharge [7]. The Li III line (13.5 nm) is used to monitor the lithium content into the plasma.
The LLL is preheated at about 220 °C (melting point T=186 °C) in a separate volume and then inserted from one vertical port in the shadow of the main toroidal limiter at a distance from the last closed magnetic surface (LCMS) that can be varied, shot by shot, between 0 and 4 cm.

3. Experimental Results of Lithization

The possibility to change, shot by shot, the distance of LLL from the LCMS has allowed both to investigate the Li effects on the plasma performance and also to assess the limits of the present LLL configuration in terms of overheating, admissible evaporation rate and CPS resistance to the damage. In the first experiments started at the end of 2005, the liquid lithium limiter has been used mainly as an active source for depositing a thin Li film on the inner wall during plasma discharges (lithization) [1]. With respect to un-lithizated discharges with

similar plasma parameters, a relevant reduction of particle recycling, of Z_{eff} and of radiation losses is observed, the edge electron temperature, increases by more than 50% and the MHD edge activity is nearly suppressed [1,8,9]. Whether the LLL, after lithization, is completely extraxted or is kept in the vessel, at a distamce from the LCMS larger than 2.0 - 2.5 cm makes hardly any difference , except for the film duration which is longer when LLL stays in. On the contrary, when the LCMS - LLL distance is reduced to less than 2.0 cm a different phenomenology develops and the LLL surface interacts more directly with the plasma. This causes a progressively larger release of Li atoms into the plasma due to the stronger evaporation (the LLL surface temperature rises up to 500-600 °C) and physical sputtering. The clearest evidence of this is the formation of a toroidal ring of a bright green light emitted by single ionized Li atoms (λ=548.4 and 548.6 nm) at the bottom of the vacuum chamber. This radiation is found well localized at plasma periphery (r/a > 0.79) and contributes to the reduction of the thermal loads on the toroidal limiter surface [10]. In these conditions, low Z_{eff} in the central plasma and low plasma dilution have been observed.
The following section will describe the results of lithizated discharges with LLL either completely extracted or maintained well in the main limiter shadow at about 2.0 -2.5 cm from the LCMS.

3.1. Peaked density profiles

On FTU, enhanced plasma performances have been obtained in high density regimes that are characterized by very peaked density profiles with peaking factors ($n_e(0)/\langle n_e \rangle_{vol}$) up to 2.5. This transition spontaneously arises for $\bar{n}_e > 1.0 \times 10^{20} m^{-3}$ with the appearance of MARFE [11] and the formation of a high-density gradient at about r/a=0.8.
An example of these discharges is shown in fig. 2. The plot here displays the temporal evolution of the line average density, as measured by the central and peripheral interferometer chords, for two high density discharges with B_T=6T and I_p=0.5MA. Looking at the central densitiy, a first increase arises for both shots at about 0.6 s, corresponding to the onset of MARFE oscillations. The further increase of the central density for t > 0.7s up to the value of 2.8×10^{20} m^{-3} in the discharge #30583 is due only to additional gas puffing. The peaking effect is evidenced for both shots by the strong change seen on the central chord while the values of the peripheral chord remain almost unchanged and equal for both discharges. This latter observation is also confirmed by the Langmuir probe measurements that display very similar SOL electron density radial profiles for both shots, as shown in the fig.3.

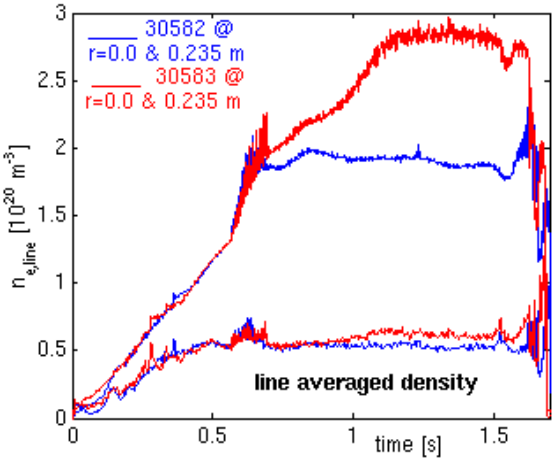

Fig. 2. *Time evolution of the central and peripheral electron density for shot 30582 in blue and shot 30583 in red*

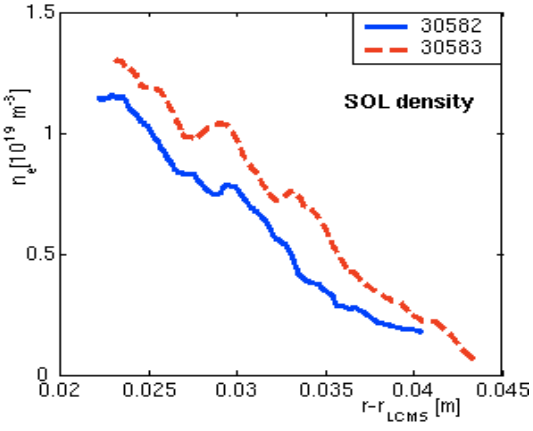

Fig. 3. *SOL density profile for the shots of Fig. 2*

To better assess the lithium effects, a comparison between boronized and lithizated discharges with I_p=0.5-0.8 MA, B_T=6.0-7.1T and increasing electron density, has been performed with the high resolution FTU scanning interferometer [3]. Particular care has been taken in the reconstruction of the density profile in presence of a MARFE. Chords that cross the MARFE region – typically on the high field side - have been excluded because of the associated well-known local density perturbation. In fig. 4 the central density evolution as a function of the volume averaged density is shown for discharges at I_p=0.5MA, B_T=6T, that are characterized by a strong density peaking. No main differences can be observed between boronized and lithizated discharges both in presence of MARFE and without it, at least up to $\langle n_e \rangle_{vol} \approx 1.5 \times 10^{20}$ m^{-3}.

Boron is indeed another very low Z element with properties very similar to those of Li. But the figure shows that only with lithium it is possible to operate at higher $\langle n_e \rangle_{vol}$ and with density peaking factor $n_e(0)/\langle n_e \rangle_{vol}$ as high as 2.5, in a regime not accessible with boron. The complete set of data in the Hugill plot is shown in fig. 5 for different plasma currents and magnetic fields, in lithizated (red) and boronized (black) conditions. The discharges developping a MARFE are represented by full symbols. From the figure it is possible to see that the Greenwald density limit, which is marked on the plot by a dashed line, has been exceeded only for discharges with an edge safety factor $q_a > 5$ ($1/q_a < 0.2$), which have lithizated walls and a well developed MARFE.

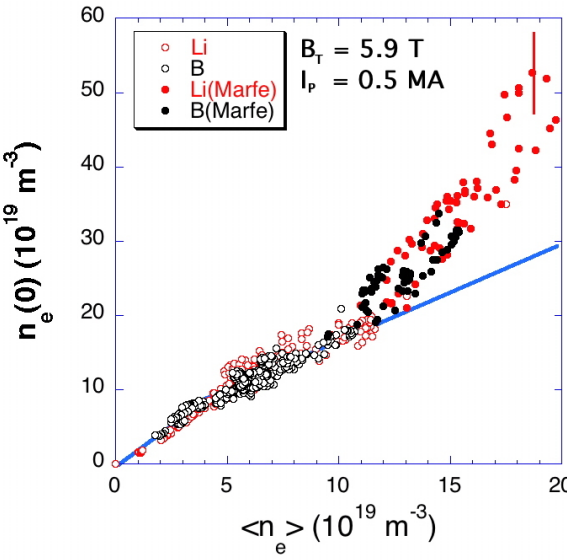

Fig. 4. Central density versus the volume averaged density, at low field and current. Red circles are used for lithium and black circles for boron conditioning discharges. Full symbols refer to discharges with well developed MARFE.

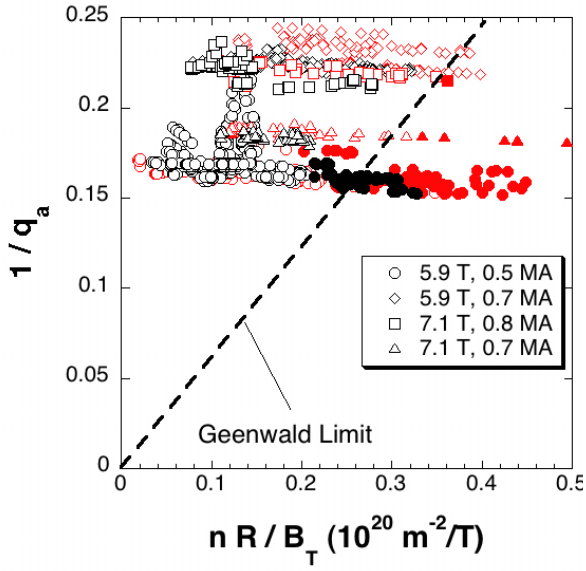

Fig. 5. Hugill plot of the discharges. Different symbols are used for different currents and magnetic field. Full symbols indicate discharges with MARFE. In red and black are indicated respectively lithizated and boronized discharges.

In particular at I_p=0.7 MA and B_T=7.1 T, q_a=5.0 by only gas puffing, the record line averaged density for FTU of 4.0×10^{20} m^{-3} has been achieved exceeding the Greenwald limit by about 30%. It is important to note that relatively high line averaged densities (up to $3.2 \times 10^{20} m^{-3}$ in a 0.47 MA, q=5.1 discharge) had already been obtained in the past under extremely clean plasma conditions but with a poloidal molybdenum limiter [12] whose contact surface was smaller (by about 10 times) than that of the present toroidal limiter. This means that both low particle recycling and low Z impurities concentration are important for the onset of MARFE and then for the density limit.

The recent experiments have allowed to upgrade the existing database [13] for the analysis of the energy transport. This database contained mainly discharges with $I_P = 0.5$ MA, $B_T = 6$ T, $\bar{n}_e = 0.6\text{-}2.8 \times 10^{20}\,m^{-3}$ and only a few discharges with higher plasma current (0.7-0.75 MA). In particular, new discharges at $I_p = 0.7$ MA and $B_T = 7.1$ T, $q_a = 5$, and line averaged density up to $\bar{n}_e = 4\times10^{20}\,m^{-3}$ have been included. The results confirm that the energy confinement time τ_E for lithizated discharges has a transition at higher values as soon as the density peaking factor overcomes the threshold value of ~1.8. This increase corresponds to a $H_{ITER97\text{-}L}$ factor as high as 1.4 to be compared with the averaged value of 0.92 associated to the old database of ohmic un-lithizated discharges. The dependence of the energy confinement time versus the linear averaged density is presented in fig. 6. Looking at the lithizated discharges at I_p=0.5 MA, B_T= 6T (triangles in light blue) it appears that the linear ohmic confinement (LOC) extends at higher values, from 54 ms up to 76 ms, that corresponds to the new saturated ohmic confinement (SOC). The same trend is also well reproduced for lithizated discharges at higher currents I_p=0.7 MA, B_T=7.1 T where the new plasma discharges, indicated by green arrows, show typical characteristics of the saturated regime.

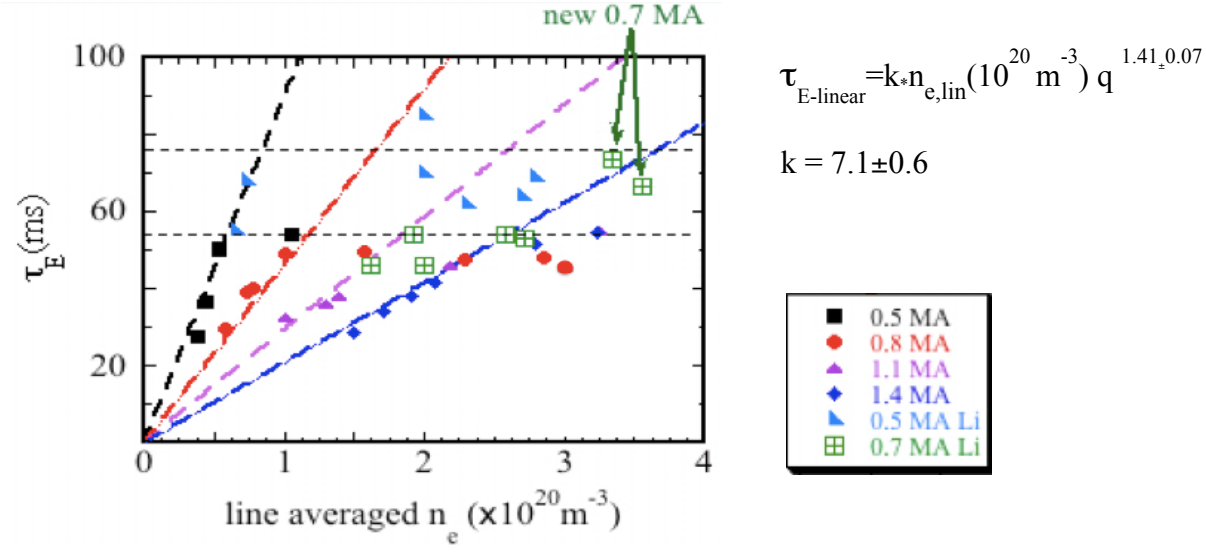

Fig. 6. *Comparison between lithizated discharges and the old ohmic database of FTU. Following the legend near the figure, lithizated discharges are indicated by the triangles in light blue at Ip=0.5MA and in green at Ip=0.7-0.75 MA, while the other symbols for different plasma current are for the un-lithizated discharges.*

The transport analysis performed with the JETTO code [14] shows that in the peaked, high-density phase, the electron thermal conductivity χ_e is about a factor 2 lower than in the un-peaked phase. Its value of ~0.2 m^2/s is typical of the saturated ohmic confinement (SOC) regime. Despite this low value, the heat transport remains dominated by the electron conductivity, being the ion conductivity very low (χ_i=0.2-0.3 m^2/s) and quite close to its neoclassical value. This improvement of the confinement at high density, which makes the ion transport negligible with respect to the electron one, is consistent with the stabilization of the ITG modes that is favored by the steepening of the density profiles. The role of lithium on the causes that trigger and maintain the high peaked density plasmas will be discussed in the following section.

Discussion

In order to investigate the nature of the inward particle flux observed in the core region of these highly peaked density plasmas, a detailed microstability analysis has been carried out by means of the gyrokinetic electromagnetic flux-tube code GKW [15]. A similar approach was followed for pellet injected discharges that, for many aspects, display characteristics very similar to those of high density lithizated plasmas. In pellet injected discharges it was shown that the increase of the density gradient due to the injected pellet at FTU collisionalities stabilizes the ITG driven modes reducing the transport and producing a positive feed back on the density gradient itself [16,17]. In lithizated plasmas the steep density gradient appears spontaneously as a consequence of an inward electron and deuterium flux. We have investigated the role of lithium in triggering and sustaining the above observed inward fluxes. Gradients and plasma parameters of the discharge shown in fig. 2 (#30582) have been taken at mid radius r/a=0.6 and t=0.3 s and t=0.8 s during the high density phase when the D and e^- experimental fluxes are found to change sign from inward (t=0.3 s) to outward (t=0.8 s). The particle flux remains directed inward in the core region of the plasma (r/a<0.3) at t=0.8s and later times and this non monotonic behaviour of the flux produces the observed peaking of the density. Three particle species have been retained in the study: e^-, D and Li. Although a full electromagnetic analysis has been carried out, for the above plasma parameters instabilities are found to be dominantly electrostatic. The growth rate of the linearly unstable modes at the two times is reported in Figure 7 for the ITG region of the spectrum and Figure 8 for the ETG region**.**

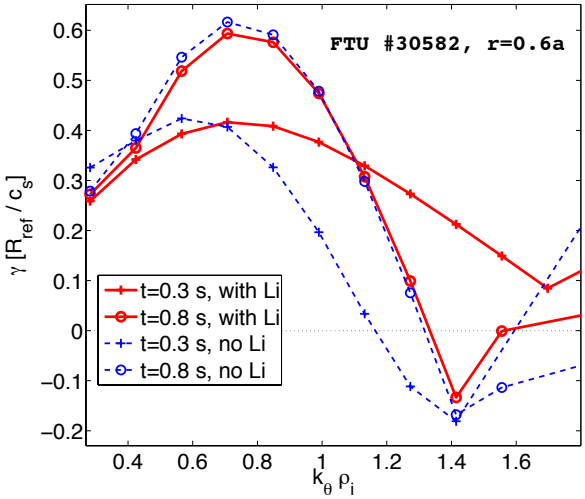

Fig. 7: Growth rates of ITG modes at two different times (cross: **t=0.3 s**, circle: **t=0.8 s**) at radial location **r=0.6a**. Results with the same physical parameters but *without* the presence of Li are also shown (blue dashed). Here $\rho_i = \rho_D$

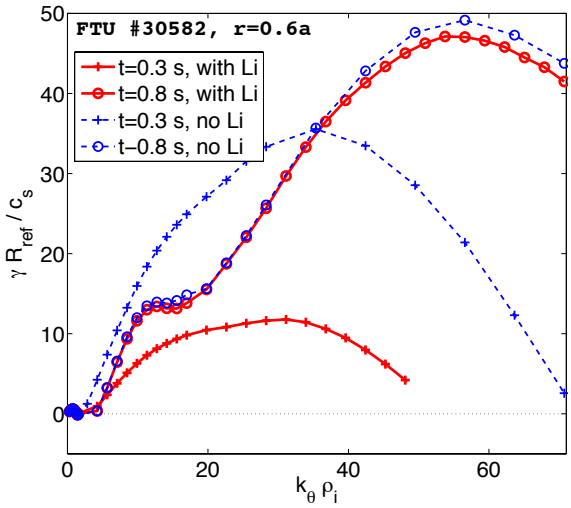

Fig. 8: Growth rates of both ITG and ETG modes at two different times (cross: **t=0.3 s**, circle: **t=0.8 s**) at radial location **r=0.6a**. Results with the same physical parameters but *without* the presence of lithium are also shown (blue dashed). Here $\rho_i = \rho_D$

The particle fluxes driven by the unstable modes are shown in figures 9 and 10 at t=0.3s and at t=0.8s.

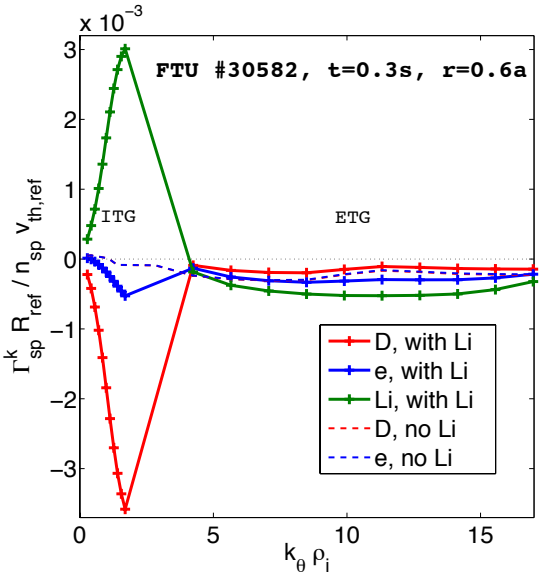

Fig. 9: Spectrum of particle flux of the three species (red: D, blue: e-, green: Li) driven by ExB convection of ITG and ETG modes at **t=0.3 s**, **r=0.6a**. Results with the same physical parameters but *without* the presence of Li are also shown (dashed lines, where D and e- fluxes coincide). The numerical values do not correspond to the saturated flux levels. Note the **different** direction of ITG driven Li flux compared to that of e- and D. The ETG driven flux is inward for all the species.

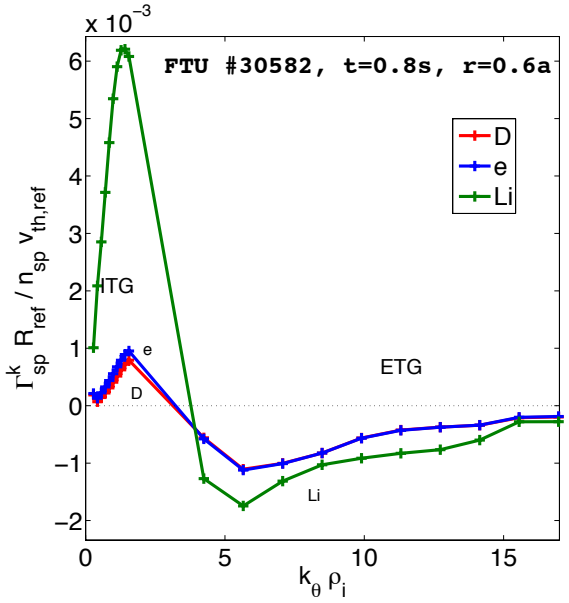

Fig.10: Spectrum of particle flux of the three species (red: D, blue: e-, green: Li) driven by ExB convection of ITG and ETG modes at **t=0.8 s**, **r=0.6a**. The numerical values do not correspond to the saturated flux levels. Note the **same** direction of ITG driven flux for Li, e- and D. The ETG driven flux is inward for all species.

As a default in linear runs, GKW applies the following normalization method: after every time step the amplitude of the potential is compared to that of the previous time step, the growth rate is calculated and stored, and then removed from the value of the fields. The time steps, therefore, can not be trivially associated with the time evolution of the solution. Once the convergence has been reached the final value of the fields is considered as an initial value of the exponential growth (or decay) which is determined by the final growth rate. As a consequence of this normalization scheme the fluxes shown in the figures above are just the initial values of the linear phase of the mode growth rate and carry no information about the saturated flux levels in the nonlinear phase. Their sign, however, does not change and determines the direction of the flux as the mode evolves.

The particle flux (linear) driven by the ETG modes is found to be inward (negative) for all the species and at both times and radial location. Particle flux driven by the ITG modes at t=0.3 s is inward for deuterium and electrons while it is outward (positive) for Lithium. The electron flux driven by ITG modes changes sign at t=0.8 s becoming outward. By comparing the sign of the linear flux with the particle flux derived from the experimental data (JETTO analysis) it appears that the flux is dominated by short wavelength ($k_\theta\rho_i\approx1.4$) ion (Lithium) temperature gradient modes at mid radius in the gradient region of the discharge. Inside one third of the minor radius, at r/a=0.3, the ITG modes are found to be stable and the inward flux is driven by ETG modes. The flux at t=0.8 s and r/a=0.3 is driven entirely by ETG modes and it is directed inward for all the particle species. The outward flux at r/a=0.6 and t=0.8 s (and later times) is driven by long wavelength ion (deuterium) temperature gradient modes ($k_\theta\rho_i\approx0.6$), while short wavelengths LiTG (Lithium gradient modes) disappear due to the reduction in Lithium concentration (Z_{eff}=1 at t>0.8s).

4. Conclusions

On FTU strongly peaked density profiles are obtained with lithium for $\bar{n}_e > 1.0 \times 10^{20} m^{-3}$ that are similar to those of pellet fuelled discharges.
This new density regime is strictly correlated with the presence of a MARFE and a strong density gradient at the plasma edge. With lithium it has been possible to extend plasma operation at very high densities and 30% beyond the Greenwald density limit at I_p=0.7 MA and B_T=7.1 T, q_a=5.0. Linear microstability analysis of these plasmas, performed with the gyrokinetic code GKW, points out the role of lithium in triggering a turbulent inward flux at mid radius for electrons and deuterium associated with the destabilization of ITG turbulence. The inward flux is sustained in the central region of the discharge by electron gradient dominated transport. The lithium flux in turn is found to be directed outward at plasma mid radius that is consistent with the low Z_{eff} value (close to 1.0) measured during the high-density phase. These results are very similar to those of pellet fuelled discharges and take advantage of the nature of the physical processes that sustain these highly peaked density plasmas.

Acknowledgements

This work was supported by the Euratom Communities under the contract of Association between EURATOM/ENEA. The views and opinions expressed herein do not necessarily reflect those of the European Commission. The authors are indebted to I. Lyublinski, A. Vertkov and A. Alexeyev for the support to LLL operations.

References

[1] APICELLA, M.L., et al, J. Nucl. Materials **363–365** (2007) 1346–1351
[2] APICELLA, M.L., et al, Fus. Eng. Des. **75-79** (2005), 351.
[3] TUDISCO, O., et al. presented to the 2nd NIFS-CRC Symposium on Plasma Surface Interactions 2010 to be published on Fus. Eng. Des. **85** (2010), issue 6
[4] MAINGI, R., et al.36th EPS Conference on Plasma Phys. Sofia, June 29 - July 3, 2009 ECA Vol.**33E**, P-2.175 (2009)
[5] MAZZITELLI, G., et al. presented to the 2nd NIFS-CRC Symposium on Plasma Surface Interactions 2010 to be published on Fus. Eng. Des. **85** (2010), issue 6
[6] LAZAREV, V.B., et al., 30th Conf. On Con. Fus. Pla. Phys., ECA2003, v.27A, P - 3.162.
[7] ALEKSEYEV, A., et al. 33rd EPS Conf. on Plasma Phys. Rome, 19-23 June 2006 P1.162
[8] MAZZITELLI, G., et al. *Fusion Energy 2006*, Vienna, 2007. Int. Atomic Energy Agency(paper IAEA-CN-116/EX/P4-16). Proc. 21st Fus. Energy Conf. Chengdu, China, 16-21 Oct. 2006.
[9] PERICOLI RIDOLFINI, V., et al. Plasma Phys. Control. Fusion **49** (2007) S123-S135
[10] APICELLA, M.L., et al., 37th EPS Conf. on Plasma Phys. Dublin 21-25 June 2010 P2.114
[11] LIPSCHULTZ, B., J. of Nucl Material **145-147**(1987) ,15
[12] FRIGIONE, D., et al. Nuclear Fusion, Vol.36, No. 11 (1996)
[13] TUCCILLO, A.A., et al, Nuclear Fusion, 49 (2009) 104013
[14] CENACCHI, G., TARONI, A, in Proc. 8th Comp. Phy., Computing in Plasma Physics, Eibsee 1986, (EPS 1986), Vol 10D, 57
[15] PEETERS, A., *et al.*, Computer Physics Communications **180**, 2650, 2009
[16] ROMANELLI, M., et al, (2004), Phys. Plasmas **11** (8), 3845
[17] ROMANELLI, M., et al, (2006), Nucl. Fusion **46** (2006) 412–418